Numerical study of the faithful replication of micro/nanostructures on curved surfaces by the electrohydrodynamic instability process

Li, Hefu; Yu, Weixing; Wang, Taisheng; Liu, Zhenyu; Desmulliez, Marc Phillipe Yves

Published in:
Electrophoresis

DOI:
10.1002/elps.201600192

Publication date:
2017

Document Version
Peer reviewed version

Numerical study of the faithful replication of micro/nanostructures on curved surfaces by the electrohydrodynamic instability process

Hefu Li[1], Weixing Yu[2,*], Taisheng Wang[3], Zhenyu Liu[3], M. P. Y. Desmulliez[4,*]

[1]School of Physical Science and Information Technology, Liaocheng University, Liaocheng, Shandong 252000, P.R. China

[2]Key Laboratory of Spectral Imaging Technology, Xi'an Institute of Optics and Precision Mechanics, Chinese Academy of Sciences, No.17, Xinxi Road, Xian 710119, P. R. China. E-mail: yuwx@opt.ac.cn

[3]State Key Laboratory of Applied Optics, Changchun Institute of Optics, Fine Mechanics & Physics, Chinese Academy of Sciences, No.3888, Dongnanhu Road, Changchun, Jilin, P.R. China

[4]MIcroSystems Engineering Centre (MISEC), Institute of Signals, Sensors and Systems, School of Engineering & Physical Sciences, Heriot-Watt University, Edinburgh EH14 4AS, UK. E-mail: m.desmulliez@hw.ac.uk

keywords: Curved surfaces/Electrohydrodynamic instability/Finite element method/micro/nanostructures /Two-phase flow

Abbrevitions: EHDIP, electrohydrodynamic instability patterning; FWHM , full-width half-maximum

Received: MONTH DD, YYY; Revised: MONTH DD, YYY; Accepted: MONTH DD, YYY

This article has been accepted for publication and undergone full peer review but has not been through the copyediting, typesetting, pagination and proofreading process, which may lead to differences between this version and the Version of Record. Please cite this article as doi: 10.1002/elps.201600192.

Abstract

This article reports the numerical study of the one-step faithful replication of micro/nano-scale structures on a fiber surface using the electrohydrodynamic instability patterning (EHDIP) process. By employing a rigorous numerical analysis method, conditions are revealed under which the faithful replication of a pattern can be achieved from a curved master electrode. It is found that the radius of curvature of the fiber plays an important role in determining the final morphology of the pattern when the destabilizing electric field is dominant in both the flat and patterned template cases. In general, stronger electric fields and larger radii of curvature of the substrate are favorable for the faithful replication of the pattern. In addition, theoretical analysis shows that higher aspect ratio micro/nanostructures can be obtained on curved surfaces by using a master with a much lower aspect ratio. The results demonstrated in this work aims to provide guidelines for the faithful fabrication of micro/nano-structures on curved surfaces by the EHDIP process.

1 Introduction

During the past decade, many experimental [1-12] and theoretical studies [13-29] have been dedicated to understand the so-called electrohydrodynamic instability patterning (EHDIP) process as this process holds the potential to generate arrays of self-organized or customized periodic micro/nanostructures. In contrast to the dewetting process that cannot easily be altered since it is driven mostly by the material properties, the EHDIP method provides a facile and flexible control over the structure formation where a variety of morphologies such as columns, channels, cavities, and holes can be produced under different conditions. Similar to the dewetting technique, the application of a laterally varying electric field distribution generated by using a topologically structured electrode was also demonstrated for the fabrication of microstructures with resolution at the nanometer scale [4]. Many natural biomaterials have hierarchical surface structures, which are of critical importance for their biological functions; super-hydrophobicity being one of the prime examples [30-32]. Surfaces from nature are very often non planar and the recent advances in the fabrication and characterization of micro/nano devices using the EHDIP process have renewed theinterest in studying the instabilities of thin films on curved surfaces as they exhibit features distinct from those on planar surfaces. On flat surfaces the electric field engenders columns or channels-like structures on the film. In contrast, on the curved surface, the force generated by the surface tension created by the radial curvature, thereonwards called the radial curvature force, acts as a destabilizing influence. Its strength

measured relative to electric field determines which final morphologies will be formed, which include beads, ridges, or both. Instability of a film on curved surfaces can produce more interesting three-dimensional hierarchic structures. Figure 1 shows a schematic diagram of a thin film deposited on a fiber under the influence of spatially varying electric fields. The instability of a thin film is initiated by the radial curvature force and the electrostatic force, whereby some interesting surface patterns can be generated [33-34]. So far, only the pattern characteristics in a film deposited on the surface of a fiber under a uniform electric field generated by a flat electrode have been researched.

This article is organized as follows. With the help of 2-D nonlinear numerical simulations, the fabrication of micro/nanostructures and hierarchical structures on curved surfaces under the influence of spatially varying electric fields is discussed. A topographically patterned electrode is employed to induce a periodic electrostatic field distribution. The control of the electric field produces a rich variety of ordered columnar structures such as cone-shape and hierarchical structures. Through numerical simulation, it is shown that three representative types of multilevel structures can be obtained. The influence of the radius of the fiber, the radial curvature force and electric field on the final morphology is investigated. In this case, the influence of the radius of curvature is relatively small so that it is easier to control the customized pattern formation process by simply controlling the intensity of the applied electric field. Indeed, experiments have shown a facile manipulation of structures by employing topographically patterned electrodes [35]. These preliminary results show the great potential of the EHDIP technique for the fabrication of customized micro- and nanostructures on curved surfaces.

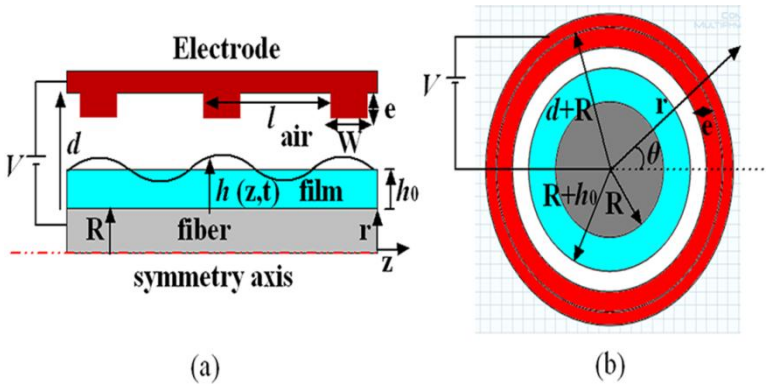

Figure 1. Schematic diagram of a liquid film coated on a cylindrical fiber with radius of R. The initial film thickness and local film thickness are denoted by h_0 and h(z, t), respectively. An electric field of voltage V is applied between the electrode and the fiber separated by a distance d. The height of the electrode protrusions, the width of the electrode protrusions, and the period of the grating mask are denoted by e, w and l, respectively. (a) front view; (b) lateral view.

2 Mathematical modeling

2.1 Problem formulation

Figure 1 shows a schematic diagram of a dielectric liquid film resting on the surface of a solid cylindrical fiber. A voltage V is applied between the cylinder and the patterned electrode. The height and width of the electrode protrusions, and the period of the grating mask are denoted by e, w and l, respectively. The dielectric constant of the film is ε. During the patterning process, the polymer film, heated to a temperature above its glass transition temperature, is treated as a viscous fluid. Let R denote the radius of the fiber, h_0 the thin film thickness before wrinkling and d the distance between the outer electrode and the fiber. In general, the evolution equation for liquid-air interface is derived under the lubrication approximation. Using the cylindrical polar coordinate system (r, ϑ, z), where the z-axis is aligned along the axis of the fiber, the continuity equation, the long-wave z and r components of the equations of motion for the film, v_z and v_r, can be

expressed as

$$-\frac{\partial P}{\partial z}+\frac{\mu}{r}[\frac{\partial(r(\partial v_Z/\partial r))}{\partial r}]=0 \quad (1)$$

$$-\frac{\partial P}{\partial r}=0 \quad (2)$$

which, together with kinematic equation for the interface,

$$\frac{\partial h}{\partial t}+v_z\frac{\partial h}{\partial z}=v_r \quad (3)$$

lead to the following evolution equation for the liquid-air free surface:

$$\begin{aligned}&\frac{\partial h}{\partial t}+\frac{\partial}{\partial z}[\frac{p_z}{\mu}(\frac{5R_c^3}{18}-\frac{R_cR^2}{2}-\frac{R_c^3}{3}\ln[\frac{R_c}{R}])]\\&+\frac{p_{zz}}{4\mu}(-\frac{13R_c^3}{36}+R_cR^2+\frac{R^4}{4R_c}+\frac{R_c^3}{3}\ln[\frac{R_c}{R}])=0\end{aligned} \quad (4)$$

Where $R_c = R+h$ is the combined thickness of the film and fiber, h is the film thickness after perturbation, μ is the viscosity of the polymer film. P_z and P_{zz} are the first and second partial derivatives of the total pressure P in the film with respect to z, respectively. The total pressure P includes four contributions: the atmospheric pressure P_0, the Laplace pressure P_{Lap}, the electrostatic pressure P_{el}, and the disjoining pressure P_{dis} such that [33]

$$\begin{aligned}&P=P_0+P_{Lap}+P_{el}+P_{dis}\\&=P_0-\gamma(\frac{\partial^2 h}{\partial z^2}-\frac{1}{R_c})+\frac{\varepsilon_0\varepsilon(\varepsilon-1)U^2}{2(R_c)^2(\ln[R_c/R]+\varepsilon\ln[d/R_c])^2}\\&+\frac{A}{6\pi h^3}+\frac{3B}{(d-R_c)^4}\end{aligned} \quad (5)$$

Where A and B denote the Hamaker constant and Born repulsion coefficient, respectively and γ is the surface tension. The destabilizing radial curvature force γ/R_c together with the electrostatic force is the dominant driving force expected to break the liquid film into an array micro/nanostructures.

2.2 Numerical method

In this work, the Level Set Two-Phase Flow application and electrostatic modules in COMSOL™ Multiphysics simulation software package are adopted to simulate the EHDIP process [36-37]. The conservative level set method is an interface tracking method, which is used for computing multiphase flow problems. The interface between fluids (gas and liquid) is represented by the 0.5 contour value of the level set function ϕ whose range is between 0 and 1. A smeared out Heavisides function is chosen such that ϕ < 0.5 for one phase, ϕ > 0.5 for the other and the transition is varied smoothly across the interface. The level set equation is expressed as:

$$\frac{\partial \phi}{\partial t} + \mathbf{U} \cdot \nabla \phi = \tau \nabla \cdot (\alpha \nabla \phi - \phi(1-\phi)\frac{\nabla \phi}{|\nabla \phi|}) \quad (6)$$

Where τ is the stabilization parameter. The parameter α controls the interface thickness and should have the same order as the computational mesh size of the elements where the interface propagates; ***U*** is the velocity vector of the interface, which can be solved by the Navier-Stokes (NS) momentum and continuity equations given by (7) and (8), respectively.

$$r\frac{\P \mathbf{U}}{\P t} + r(\mathbf{U} \cdot \nabla)\mathbf{U} = -\nabla P + \nabla \cdot (m\nabla \mathbf{U}) + \mathbf{F} \quad (7)$$

$$\frac{\partial \rho}{\partial t} + \nabla \cdot (\rho \mathbf{U}) = 0 \quad (8)$$

Here ρ is the density, μ is the viscosity and P is pressure. ***F*** is the volume force caused by the atmospheric pressure P_0, the surface tension $\boldsymbol{F}_{st}=\sigma\kappa\delta\boldsymbol{n}$, and the electrostatic pressure is P_{el}. $\boldsymbol{F}=(p_0+\sigma\kappa+p_{el})\delta\boldsymbol{n}$, where σ is the surface tension coefficient (N/m), κ is the curvature, δ is a delta function concentrated to the surface, and ***n*** is the unit outward normal to the interface. δ smoothens the surface tension, which is concentrated at the interface between fluids and is approximated according to the equation,

$$\delta = \left|\nabla\phi\right|\left|\phi(1-\phi)\right| \tag{9}$$

The interface normal vector modulus and the interface curvature are determined by Eq. (10) and Eq. (11) respectively,

$$\boldsymbol{n} = \frac{\nabla f}{\left|\nabla f\right|} \tag{10}$$

$$\kappa = -\nabla\cdot(\frac{\nabla\phi}{\left|\nabla\phi\right|}) \tag{11}$$

In order to realize the level set equations containing curvature in 2D axisymmetric coordinate, the curvature is corrected by [38]:

$$\kappa = \frac{\phi_{rr}\phi_z^2 + \phi_{zz}\phi_r^2 - 2\phi_{rz}\phi_r\phi_z}{\left(\phi_r^2+\phi_z^2\right)^{3/2}} + \frac{\phi_r}{r\sqrt{\phi_r^2+\phi_z^2}} \tag{12}$$

Where ϕ_r is the first derivative of ϕ with respect to r, ϕ_z is the first derivative of ϕ with respect to z, ϕ_{rr} is the second derivative of ϕ with respect to r, ϕ_{zz} is the second derivative of ϕ with respect to z,and ϕ_{rz} is the second derivative of ϕ with respect to r and z.

The density and viscosity are calculated from

$$\rho = \rho_1 + (\rho_2 - \rho_1)\phi \tag{13}$$

$$\mu = \mu_1 + (\mu_2 - \mu_1)\phi \tag{14}$$

Where ρ_1 and ρ_2 are the fluid densities of the air and polymer film; μ_1 and μ_2 indicate the dynamic viscosities of the air and the polymer film. The electric field is solved using the Laplace's equation for the voltage assuming that there is zero free charge in the bulk fluid:

$$\nabla\cdot\nabla V = 0 \tag{15}$$

The electrostatic pressure can be described by the following equation:

$$p_{el} = -0.5\varepsilon_0\varepsilon_p(\varepsilon_p - 1)E_p^2 \quad (16)$$

Figure 2 shows the geometry, boundary conditions and mesh of the two-dimensional model. Without loss of generality, only four periods of the pattern on the master electrode are shown here. For a patterned electrode, a DC voltage is applied between the bottom (boundary 3) and the top electrode with electrical potential (boundaries 7, 8, 9…21, 22 and 23). The boundary conditions for the fluid flow are: (a) no slip at boundaries 3, 7, 8, 9…21, 22 and 23; (b) periodic boundary on boundaries 1, 2, 4 and 6; (c) initial fluid interface at boundary 5. In order to simulate a periodic structure, it is necessary to introduce periodic boundary conditions at boundaries 1, 2, 4 and 6. The sources 1 and 3 corresponding to the destinations 4 and 6, respectively. The expressions for the sources are the pressure in the fluid *P* and the flow velocity ***U***. Two-phase flow is in the form of conservative level set. Properties of the polymer liquid used in the simulation are presented in Table 1.

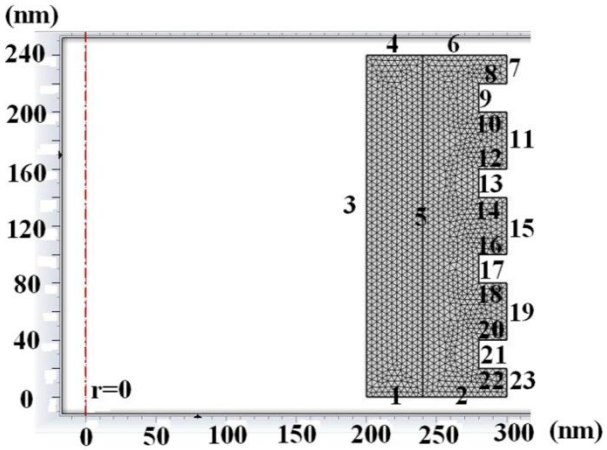

Figure 2. Schematic diagram introducing the geometry, boundary conditions and mesh of the two-dimension model in 2D axisymmetric coordinate.

Table 1. Properties of the material used in the numerical simulations.

Simulated dynamic viscosity (*Pa·S*)	Density (kg/m^3)	Dielectric constant	Surface tension (N/m)
1	1000	2.5	0.038

3 Results and discussions

3.1 Numerical result of the faithful replication of the patterned electrode

The detailed time evolution of the EHDIP process on the fiber surface with a patterned template is shown in Figure 3. Simulation results show a two-dimensional periodic microstructure induced by a patterned electrode with protrusion height and width of 20 nm. The period *l* of the protrusion is 60 nm and the radius of the fiber is 200 nm. The gap *d* between the electrodes is 100 nm. The initial polymeric film thickness is 40 nm. The applied DC voltage on the top electrode is 150 V and the bottom electrode is grounded. Initially the polymer film surface is flat as shown in Figure 3(A). As the spatial heterogeneity of the electrostatic field is introduced by the patterned top electrode, the polymer liquid grows upwards firstly under the protrusions of the top electrode due to the higher electric field in those areas as shown in Figure 3(B). The resulting uplifted polymer experiences a greater electrostatic force as the polymer approaches the top electrode, pulling the polymer fluid further towards the protrusion of the top electrode as shown in Figure 3(C). The growing polymer touches the surface of the top electrode and is stopped from moving further upwards as indicated in Figure 3(D). Instabilities in the film on the fiber under a spatially varying electric field are shown here to engender ordered micro/nanostructures. In this particular case, nanostructures with width of around 28 nm (full-width at half-maximum) and depth of 80 nm can be created.

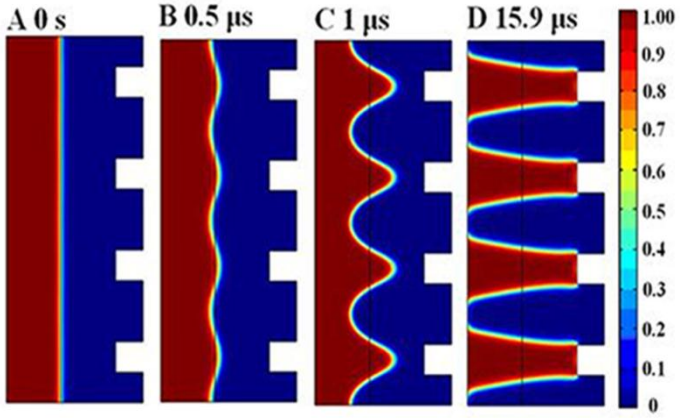

Figure 3. Spatiotemporal evolution of a 40 nm thick polymer liquid interface on fiber with radius 200nm. The height *e* of the electrode protrusions, the width *w* of the electrode protrusions, and the period *l* of the grating mask are 20 nm, 20 nm and 60 nm, respectively. The applied voltage is 150 V and the gap *d* between the electrodes is 100 nm. Red color represents the polymer liquid, and the blue color represents air.

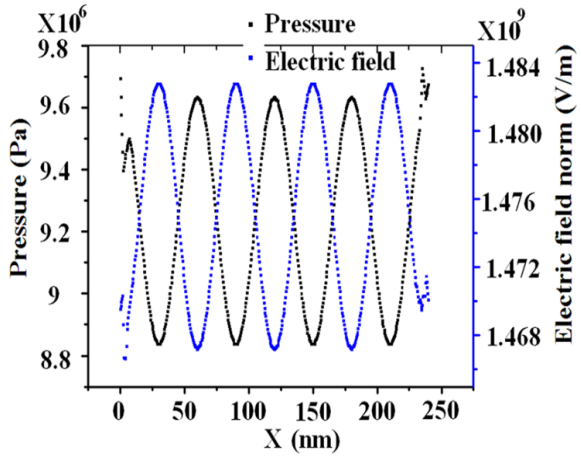

Figure 4. Electrostatic field distribution and pressure distribution on the surface of the film at the initial stage. The broken black line is used to characrerize the the initial pressure located at the surface of the polymer film. The broken blue line is used to characrerize the initial electric field strength located at the surface of the polymer film.

Figure 4 shows the diagram of pressure and the electric field strength distribution at the film surface at the initial stage as shown in Figure 3(A). Both the electric field distribution and the pressure distribution follow a sinusoidal profile.

The electric field strength underneath the center of the protrusion is much larger than in other areas, such that a larger electrostatic force is exerted on the film surface. Accordingly, the internal pressure in this region is lower than in other areas as seen in Figure 4. Figure 3 shows the volume fraction of air. While the position of the air-polymer film interface appears clearly, one can obtain an even sharper interface by plotting the 0.5 level of the same quantity using a filled contour plot in order to characterize the dimension of the nanostructures. This type of filled contour plot is adopted in the following figures.

3.2 Fabrication of three characteristic hierarchical patterns

As with many biological surfaces, hierarchical patterns on curved surfaces are the basis for the formation of super-hydrophobic or self-cleaning surfaces. Therefore, simulation results concerning three characteristic hierarchical patterns formed on curved surfaces are shown. Figure 5 shows the nonlinear evolution of a polymer film with thickness 30 nm on the fiber with radius 100 nm under a patterned top electrode with pattern periodicity 100 nm. The width and the height of the downward protrusions of the patterns shown in the top electrode are 60 nm and 30 nm, respectively. The applied voltage is 200 V and the gap between the electrodes is 100 nm. A similar growth pattern as in Figure 3 can be seen, except for the growth of a secondary grating, which is composed of both small humps of 12 nm wide (full-width half-maximum FWHM) and 14 nm high and larger structures of 30 nm FWHM and 70 nm height as shown in Figure 5(E). These composite columns grow toward the top electrode. This behavior arises from the onset of a larger electrostatic force difference emerging at the boundaries of the polymer columns. The polymer material at the boundaries is rapidly depleted, leaving residual polymer between the columns as shown in Figure 5(C). As the process is developing, the residual polymer forms small humps, hence the multilevel structures obtained in one step as shown in Figure 5(D-E).

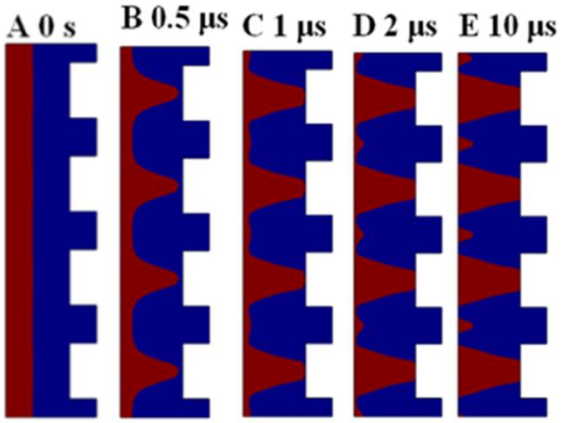

Figure 5. Spatio-temporal evolution of a 30 nm thick polymer liquid interface on the fiber with radius of 100 nm. The height *e* of the electrode protrusions, the width *w* of the electrode protrusions, and the period *l* of the grating mask are 30 nm, 60 nm and 100 nm, respectively. The applied voltage is 200 V and the gap *d* between the electrodes is 100 nm. Red color represents the polymer liquid, and the blue color represents air.

Figure 6 shows the nonlinear evolution of a polymer film with thickness 20 nm on the fiber with radius 100 nm under a patterned top electrode with pattern periodicity of 180 nm. The width and height of the downward protrusions of the patterns shown in the top electrode are 90 nm and 30 nm, respectively. The applied voltage is 250 V and the gap d between the electrodes is 120 nm. Two small humps are grown and are located between adjacent protrusions. The image in Figure 6(E) is the snapshot of the quasi-equilibrium structures after the interface evolves for a short time but before the coalescence of the larger ridge and small humps on both sides.

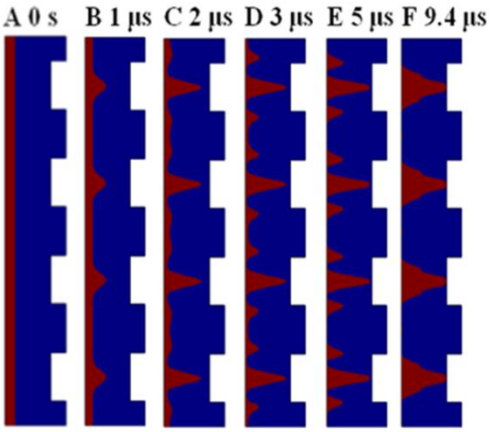

Figure 6. Spatio-temporal evolution of a 20 nm thick polymer liquid interface on the fiber with radius of 100 nm. The height *e* of the electrode protrusions, the width *w* of the electrode protrusions, and the period *l* of the grating mask are 30 nm, 90 nm and 180 nm, respectively. The applied voltage is 250 V and the gap *d* between the electrodes is 120 nm. Red color represents the polymer liquid, and the blue color represents air.

Figure 7 shows the ordering of the hierarchic nanostructures when the patterned electrode has a lower aspect ratio. The polymer film thickness is 50 nm; the fiber radius is 100 nm and the patterned top electrode with pattern periodicity of 600 nm. The width and height of the downward protrusions of the patterns shown in the top electrode are 400 nm and 20 nm, respectively. The applied voltage is 250 V and the gap between the electrodes is 150 nm. The images in this figure are also snapshots of the quasi-equilibrium structures after the interfaces evolve for a long time but before the coalescence of the adjacent structures. Experimentally, the quasi-equilibrium structures could be fixed permanently by cross-liking the polymer at this stage. Figure 7(D) shows a pair of larger columns and one small hump formed under each protrusion. A pair of small humps is formed between adjacent protrusions in the master electrode. The high electric field strength under the protrusions reduces the length scale of the instability locally and thus produces the three ridges under each protrusion while a larger electrostatic force difference exists at the boundaries of the polymer columns, resulting in the formation of two small humps under the cavity.

In summary, we have demonstrated through simulations that three characteristic hierarchical patterns can be obtained by a proper control of EHDIP process parameters. It is found that the final multilevel morphology is determined by the initial film thickness, electrode spacing, distance of the electrode protrusions, aspect ratio of the electrode protrusion. All above characteristic hierarchical patterns can be attributed to the spatially over-modulated process where features of the template pattern cannot be faithfully transferred into polymer, which is an undesirable feature of the process for the normal micro/nano-replication process [39]. In these three over-modulated processes, two critical conditions must meet. One is the mass parameter γ, i.e. the ratio of practical mass volume on the requisite mass volume, should be less than 1 and the other is that the corresponding modified maximum unstable wavelength should be smaller than half of the characteristic length. Furthermore, in order to achieve hierarchical structures, smaller aspect ratio of the electrode protrusion is also necessary.

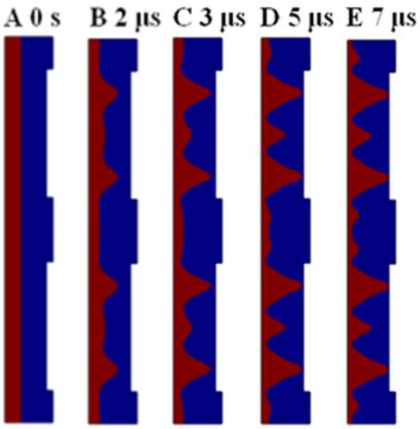

Figure 7. Spatio-temporal evolution of a 50 nm thick polymer liquid interface on the fiber with radius of 100 nm. The height *e* of the electrode protrusions, the width *w* of the electrode protrusions, and the period *l* of the grating mask are 20 nm, 400 nm and 600 nm, respectively. The applied voltage is 250 V and the gap *d* between the electrodes is 150 nm. Red color represents the polymer liquid, and the blue color represents air.

3.3 The influence of radii of curvature

The EHDIP process was simulated on fiber surfaces with different radii of curvature in order to characterize the influence of the curvature of the fiber on the final morphology of the generated structures. Results are shown in Figure 8. In the simulation, the polymer film is 200 nm thick, the gap between the electrodes is 460 nm and the applied voltage is 550 V. The radii of curvature for the cases of Figures A to E are 200 nm, 500 nm, 700 nm, 1μm, 10 μm, respectively. Figure 8(A) shows an array of cone like structures in the thin film rested on a thin fiber with a 200 nm radius. In this case, there is still some residual film in the areas between the cone structures, which means the film is not completely depleted. The radial curvature force plays an important role in maintaining the stabilization of the film against the electrostatic force and therefore has a negative contribution to the nanostructures formation. When the radius of the fiber is increased to 500 nm as shown in Figure 8(B), four higher ridges are formed under the flat electrode so that the film is nearly depleted in the areas between the ridges. The period of the formed ridge structures is the same as in Figure 8(A). Furthermore, when the fiber radius is increased to 700 nm as shown in Figure 8(C), four ridges are still formed in the film but the middle two ridges are shifted towards the center point. This shift becomes more pronounced when the radius of curvature is increased to 1 μm as shown in Figure 8(D). In this case, the outer two ridges have a little shift towards the center point as well. In addition, the width of the outer two ridges also becomes larger. Finally, when the radius of curvature is dramatically increased to 10 μm, the middle two ridges have merged into one single column. At the same time, the outer two ridges have grown into two thicker columns as shown in Figure 8(E). In this case, the three columns are also periodically with a period larger than in Figures 8(A) and 8(B). In general, smaller radii of curvature help improving the resolution of the formed structure but, in some cases, non-periodic and hierarchic structures can be formed.

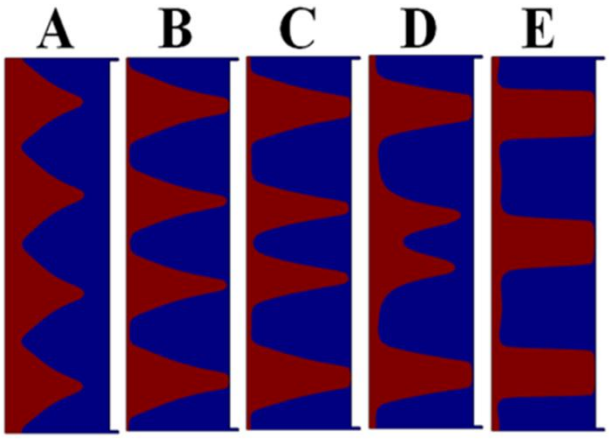

Figure 8. Spatio-temporal evolution of a 200 nm thick polymer liquid interface deposited on a fiber with different radii. The applied voltage is 550 V and the gap between the electrodes is 460 nm. Red color represents the polymer liquid, and the blue represents air.

Figures 9(A) to 9(F) show the formation of structures for a polymer film of 40 nm thickness induced by a flat template with applied voltage of 100 V. The gap between the electrodes is fixed at 80 nm. In the case of a radius of curvature of 50 nm as shown in Figure 9(A), there are four ridges formed with the middle two ridges about to merged together. As the radius of curvature is increased to 60 nm as shown in Figure 9(B), five ridges are formed but still not distributed periodically. Furthermore, for a radius of 100 nm or larger as shown in Figures 9(C) to 9(F), standard periodic structures are formed with a conic shape, and then with a columnar shape thereafter. Smaller radii of curvature have a stronger impact in maintaining the stabilization of the film, making it difficult for the electrostatic force to destabilize the film. As the radius of curvature decreases the electrostatic force is more prominent and therefore dominates the EHDIP process.

More simulation results show that, for patterned electrodes, the faithful replication of the top electrode pattern is only obtained when the applied gradient driven flow wins over the spinodal flow based on the characteristic length scale. Thus, in general, the final morphology depends on the fiber radius *R* as well. Figure 10 shows the simulation results of

EHDIP process under different radii of curvature when a patterned electrode is used. As can be seen from Figure 10(A), when the radius of the fiber is 50 nm, the pattern on the electrode cannot be replicated faithfully. As the radius of the fiber is increased to 100 nm, the periodic pattern is well replicated into the polymer. For *R*=1 μm as shown in Figure 10(D), columnar shape structures are obtained with steep sidewall and large aspect ratio of 2.5. In summary, the large number of simulations carried out in this study all point to a general conclusion that a small radius of curvature force is unfavourable for the faithful replication of the patterned template. Figure 11(A) shows the diagram of pressure distribution at the film surface at the initial stage as shown in Figure 10. The pressure distribution follows a sinusoidal profile and the influence of the radius of the fiber on the mean pressure. With the increase of the fiber radius, the mean pressure decreases as shown in Figure 11(B).

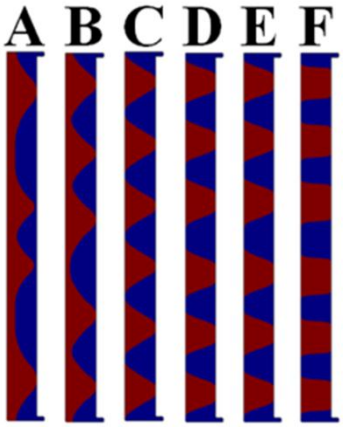

Figure 9. Simulations for a 40 nm thick when (a) R= 50 nm, (b) R=60 nm, (c) R=100 nm, (d) R=200 nm, (e), R=1μm, (f), R=5μm. The applied voltage is 100 V, the electrode distance is 80 nm. Red color represents the polymer liquid, and the blue colour represents air.

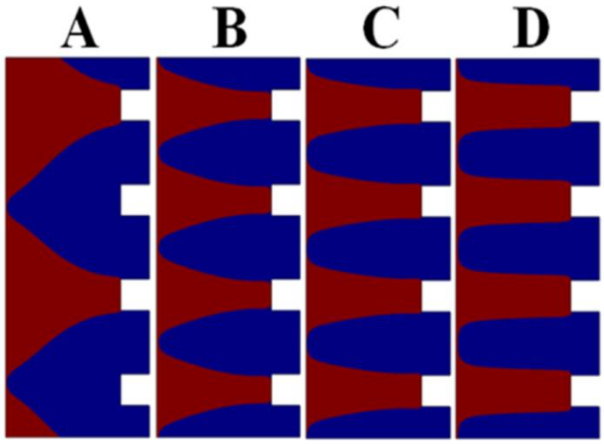

Figure 10. Simulations for a 40 nm thick when (a) R= 50 nm, (b) R=100 nm, (c) R=200 nm, (d) R=1 μm. The applied voltage is 123 V, the electrode distance is 100 nm and the width and height of the patterned template are the same at 20 nm. The period of the patterned template is 60 nm. Red color represents the polymer liquid, and the blue colour represents air.

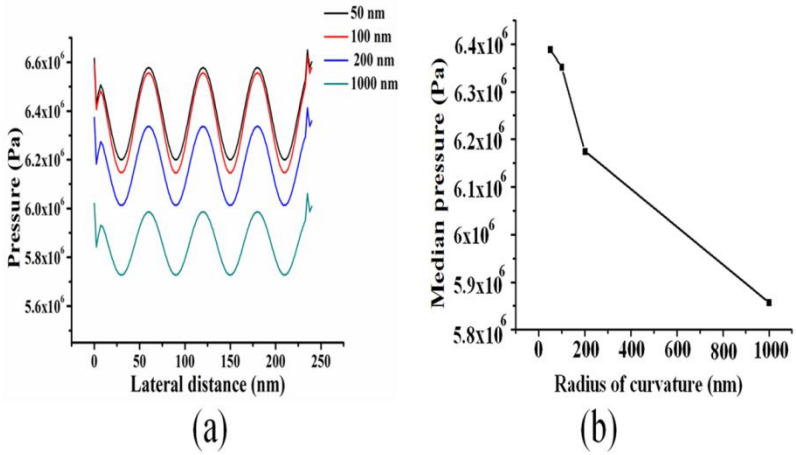

Figure 11. (a) Initial pressure located at the surface of the polymer film as shown in Figure 10, (b) Relationship between the median pressure and the radius of curvature.

4 Concluding remarks

In summary, we have demonstrated through rigorous numerical simulations that customized micro/nanostructures can be successfully obtained on curved surfaces by using the EHDIP process. It is found that the final surface morphology is

sensitive to the curvature radius of the fiber when the destabilizing electric field is dominant. In order to achieve the faithful fabrication of the customized patterns on the master, a large radius of curvature of the substrates as well as stronger electric voltages are favorable. The fabrication results show that microstructures with large aspect ratio can be achieved by using a master with a low aspect ratio, which indicates the great advantage of the EHDIP process in terms of savings in fabrication costs and time in producing a master with such characteristics. The results reported in this work provide a good guidance for the fabrication of micro/nanostructures on curved surfaces by using the EHDIP process, which has the great potential to fabricate micro/nanostructures with hierarchical shapes.

The authors acknowledge the financial support from Natural Science Foundation of China under grant numbers 61475156, 61361166004 and 90923036. The financial support of the UK Innovative electronic Manufacturing Research Centre (IeMRC) is also acknowledged through the funding of the Flagship project "Smart Microsystems" (FS/01/02/10).

The author has declared no conflict of interest.

5 References

[1] Erik Schaeffer, Thomas Thurn-Albrecht, Thomas P. Russell, Ullrich Steiner, *Nature*. 2000, *403*, 874-877.

[2] Paru Deshpande, Xiaoyun Sun, Stephen Y. Chou, *Appl Phys Lett*. 2001, *79*, 1688-1690.

[3] Stephen Y. Chou, Lei Zhuang, Linjie Guo, *Appl phys Lett.* 1999, *75*, 1004-1006.

[4] Xinya Lei, Lin Wu, Paru Deshpande, Zhaoning Yu, WeiWu, Haixiong Ge, Stephen Y Chou, Nanotechnology. 2003, 14, 786-790.

[5] Stephan Harkema, Ullrich Steiner, *Adv. Funct. Mater.* 2005, *15*, 2016-2020.

[6] Nicoleta E. Voicu, Stephan Harkema, Ullrich Steiner, *Adv. Funct. Mater*. 2006, *16*, 926-934.

[7] Ning Wu, Leonard F. Pease III, William B. Russel, *Adv. Funct. Mater*. 2006, 16, 1992-1999.

[8] Narasimhan Arun, Ashutosh Sharma, Vijay B. Shenoy, K. S. Narayan, *Adv. Mater*. 2006, *18*, 660-663.

[9] Mihai D. Morariu, Nicoleta E.Voicu, Eric Schaffer, ZhiQun Lin, Thomas P. Russell, Ullrich Steiner, *Nat Mater*. 2003, *2*, 48-52.

[10] Xiaolei Xi, Dan Zhao, Fei Tong, Tingbing Cao, *Soft Matter*. 2012, *8*, 298-302.

[11] Goldberg-Oppenheimer, Sumeet Mahajan, Ullrich Steiner, *Adv. Mater*. 2012, *24*, 175-180.

[12] S. G. Pattader, Indrani Banerjee, Ashutosh Sharma, Dipankar Bandyopadhyay, *Adv. Funct. Mater.* 2011, *21*, 324-335.

[13] Lin Wu, Stephen Y. Chou, *Appl. Phys. Lett.* 2003, *82*, 3200-3202.

[14] Ruhi Verma, Ashutosh Sharma, Kajari Kargupta, Jaita Bhaumik, *Langmuir.* 2005, *21*, 3710-3721.

[15] Ning Wu, Leonard F. Pease III, William B. Russel, *Langmuir*. 2005, *21*, 12290-12320.

[16] Leonard F. Pease III, William B. Russel, *J Chem Phys*. 2006, *125*, 184716.

[17] Dipankar Bandyopadhyay, Ashutosh Sharma, *J Colloid Interface Sci.* 2007, *311*, 595-608.

[18] Jayati Sarkar, Ashutosh Sharma, Vijay B. Shenoy, *Phys Rev E.* 2008, *77*, 031604.

[19] Ning Wu, William B. Russel, *Nano Today*. 2009, *4*, 180-192.

[20] Jakob Heier, Jan Groenewold, Ullrich Steiner, *Soft Matter.* 2009, *5*, 3997-4005.

[21] P. Dinesh Sankar Reddy, Dipankar Bandyopadhyay, Ashutosh Sharma, *J. Phys. Chem. C.* 2010, *114*, 21020-21028.

[22] Ning Wu, Michail E. Kavousanakis, William B. Russel, *Phys Rev E*. 2010, *81*, 026306.

[23] Dipankar Bandyopadhyay and Ashutosh Sharma, *J. Phys. Chem. C.* 2010, *114*, 2237-2247.

[24] Cindy Y. Lau, William B. Russel, *Macromolecules.* 2011, *44*, 7746-7751.

[25] Ajoy Patra, Dipankar Bandyopadhyay, Gaurav Tomar; Ashutosh Sharma, and Gautam Biswas, J Chem Phys. 2011, 134, 064705.

[26] Kartick Mondal, Prashant Kumar, Dipankar Bandyopadhyay, *J Chem Phys*. 2013, *138*, 024705.

[27] P. Dinesh Sankar Reddy, Dipankar Bandyopadhyay, Ashutosh Sharma, J. Phys. Chem. C. 2012, 116, 22847-22858.

[28] H. Li, W. Yu, L. Zhang, Z. Liu, K.E. Brown, E. Abraham, S. Cargill, C. Tonry, M.K. Patel, C. Bailey, M. P. Y. Desmulliez, *RSC Adv*. 2013, *3*, 11839-11845.

[29] H. Li, W. Yu, Y. Wang, H. Bu, Z. Liu, Eitan Abraham, M. P. Y. Desmulliez, *RSC Adv*. 2014, *4*, 13774-13781.

[30] Ralf Blossey, *Nat Mater*. 2003, *2*, 301-306.

[31] Yewang Su, Baohua Ji, Kai Zhang, Huajian Gao, Yonggang Huang, Kehchih Hwang, Langmuir. 2010, 26, 4984-4989.

[32] Michael Nosonovsky, Bharat Bhushan, *Microelectronic Eng*. 2007, *84*, 382-386.

[33] V. Anoop Kishore, Dipankar Bandyopadhyay, *J. Phys. Chem. C.* 2012, *116*, 6215-6221.

[34] Bo Li, Yue Li, Guang-Kui Xu, Xi-Qiao Feng, *J. Phys.: Condens. Matter.* 2009, *21*, 445006.

[35] H. Li, W. Yu, T. Wang, H. Zhang, W. Niu, E. Abraham, M. P. Y. Desmulliez, *RSC. Adv*. 2014, *4*, 38379-38383.

[36] H. Tian, J. Shao, Y. Ding, X. Li, X. Li, *Electrophoresis*, 2011, *32*, 2245-2252.

[37] Y. Lin, *Electrophoresis*, 2013, *34*, 736-744.

[38] Cheng Jun-xia, Hu Xiao-mian, *Explosion and shock waves*. 2012, *32*, 150-156.

[39] Hongmiao Tian, Yucheng Ding, Jinyou Shao, Xiangming Li, Hongzhong Liu, *Soft Matter*, 2013, 9, 8033-8040.